Chemical Engineering Journal 464 (2023) 142713

Contents lists available at ScienceDirect

Chemical Engineering Journal

journal homepage: www.elsevier.com/locate/cej

Near-perfect suppression of Li dendrite growth by novel porous hollow carbon fibers embedded with ZnO nanoparticles as stable and efficient anode for Li metal batteries

Hyun-Jin Shin [a,b], Saleem Abbas [a], Jaewon Kim [a,b], Jinhan Cho [b], Heung Yong Ha [a,c]

[a] Center for Energy Storage Research, Korea Institute of Science and Technology (KIST), 14-gil 5, Hwarang-ro, Seongbuk-gu, Seoul 02792, Republic of Korea
[b] Department of Chemical and Biological Engineering, Korea University, 145 Anam-ro, Seongbuk-gu, Seoul 02841, Republic of Korea
[c] Department of Energy and Environmental Engineering, Korea University of Science & Technology (UST), 217 Gajeong-ro, Yuseong-gu, Daejeon 34113, Republic of Korea

ARTICLE INFO

Keywords:
Li metal battery
Free-standing anode
Li dendrite
Porous hollow carbon nanofiber
Electrospinning

ABSTRACT

For the practical application of next-generation Li metal batteries (LMBs), a Li metal anode with high safety and efficiency is essential. However, LMBs still suffer from the problems caused by the growth of Li dendrites at the Li metal anode. In this study, we introduce a novel way that could dramatically suppress the growth of Li dendrites and improve the performance of LMBs. A free-standing porous hollow carbon nanofiber embedded with lithiophilic ZnO nanoparticles (P-HCNF@ZnO) is fabricated using a dual-nozzle electrospinning technique followed by carbonization. The nano-sized pores formed in the shell of hollow carbon fiber provide passages for Li ions to penetrate into the core space of the hollow fiber, and the lithiophilic ZnO particles play a decisive role in inducing and plating Li ions inside the core efficiently and uniformly. Therefore, Li ions are mostly electroplated/stripped on the internal surface of the porous hollow fibers and dendrites are rarely formed on their exterior surface even under fast lithiation conditions, while numerous Li dendrites are formed on the exterior surface of the non-porous hollow fiber electrode (HCNF@ZnO). As a result, the P-HCNF@ZnO electrode exhibits a very low over-potential of about 87 mV, a stable capacity retention of about 95% at a high current density of 1.0 mA cm^{-2}, and a much higher performance than HCNF@ZnO in a symmetric cell test. Furthermore, in full cell tests, the $LiFePO_4$ (LFP) battery made of lithiated P-HCNF@ZnO anode exhibits a high capacity of 175.3 mAh g^{-1} and a lower over-potential by 0.29 V than the reference sample. Analytical works and theoretical interpretations, elucidated that the Li metal anode made of the P-HCNF@ZnO significantly improves the performance of LMBs.

1. Introduction

The global market of Li-ion batteries (LIBs) has been challenging a new goal of energy density higher than 500 Wh kg^{-1} at the cell level for various electronic applications such as smart mobile electronics, electric vehicles, and advanced energy storage systems. To reach such a high goal, Li metal is the indispensable component as anode material in the battery system, owing to its high theoretical capacity of 3,860 mAh g^{-1}, low density of 0.59 g cm^{-3}, and low redox potential of − 3.04 V (vs. SHE) [1]. For example, the Li metal batteries (LMBs) employing a Li metal anode and a high energy density cathode such as sulfur and oxygen can offer an excellent high theoretical specific energy of 2,567 Wh kg^{-1} and 3,505 Wh kg^{-1}, respectively [2,3]. However, the Li metal anode still has critical issues in practical applications, such as the growth of Li dendrites, huge dimensional changes, and poor Coulombic efficiency (CE) during cycling. The growth of Li dendrites has been considered a very challenging issue because it raises serious safety concerns and leads to poor electrochemical performance. As the Li dendrite grows, it penetrates the separator and reaches the cathode, eventually causing an internal short-circuit and a fire or an explosion. Also, they can bring about unwanted side reactions at the interface between electrode and electrolyte, resulting in the formation of unstable solid electrolyte interphase (SEI) layer, which may undergo continuous crack/reconstruction due to the volumetric changes of Li layers during plating/stripping cycles. These unfavorable side reactions are accompanied by severe electrolyte consumption of electrolyte and the formation of dead Li, eventually leading to a poor CE, rapid capacity fading, and a short life span [4,5].

Various strategies have been tried to overcome these problems, such as optimizing electrolytes, using solid electrolytes, and appropriate design of Li host frameworks. Optimizing liquid electrolytes by adding additives has been reported to form a stable SEI layer with high mechano-chemical stability. However, the additives were continuously consumed during cycling and failed to improve the stability of the

https://doi.org/10.1016/j.cej.2023.142713
Received 5 November 2022; Received in revised form 19 February 2023; Accepted 29 March 2023
Available online 1 April 2023

batteries [6,7]. Solid electrolytes may potentially suppress the formation of Li dendrites Li, but most solid electrolytes have intrinsically low ion conductivity at room temperature. Moreover, sulfide-based solid electrolytes suffer from an unstable interphase formation with active materials, including Li metal [8].

Designing Li host frameworks have recently drawn attention as a strategy for making stable Li metal anodes because the host frameworks can directly affect the nucleation behavior, particularly at the initial Li plating step. According to the heterogeneous nucleation model for the growth of Li dendrites, the initial morphology of Li nucleation substantially affects the final morphology of Li crystals, eventually affecting the electrical performance of LMBs [9–15]. Many studies have been reported on the design of Li host frameworks, such as the design of 3 dimensional (3D) conductive current collector, carbon coating on the current collector, and the introduction of a lithiophilic material to control the Li plating in the designated host space to prevent Li dendrite growth. Yang et al. [16] reported a Cu current collector with a 3D submicron-size Cu skeleton structure that could disperse the charge centers for Li nucleation to suppress the formation of Li dendrites during Li plating. Zheng et al. [17] reported a hemispherical amorphous carbon layer coating on the surface of the Cu current collector that could serve as an ideal interfacial layer to suppress Li dendrite growth and dead Li formation through the generation of stable SEI layers. Liang et al. [18] reported the fabrication of a Li metal anode prepared by coating a carbon sheet with lithiophilic silicon followed by an infusion of molten Li. Guo et al. [19] reported the lithiophilic iodine-containing polymer layer on Li metal anode can guide uniform Li plating behavior to suppress Li dendrite growth. The Li anodes showed enhanced stability and reduced volume expansion.

Although these strategies could help suppress more or less Li dendrite growth and volume expansion, there still remain fundamental side reactions and volume expansion at the anode. Furthermore, the electrode morphology continuously changes during cycling by the growth of Li dendrite and the formation of dead Li, thereby deteriorating the stability of Li batteries.

Recently, the hollow carbon frameworks embedded with lithiophilic seed materials have been in the limelight as a feasible way to serve the Li metal anode with high stability and reliability [20]. The lithiophilic seeds in the core of the hollow structure drive Li ions towards the core space, and the carbon shell guides Li plating and blocks the contact between the Li and the electrolyte; thereby, it could overcome the above-mentioned fundamental problems. Yan et al. [11] and Kim et al. [21] reported that Li plating were formed in the core spaces of hollow carbon spheres or hollow carbon fibers embedded with lithiophilic Au particles during Li plating. These studies exhibited the feasibility of fabricating stable Li metal anodes. In the case of the hollow structure frameworks embedded with lithiophilic materials suggested in the previous studies, the shell of the hollow carbon structures may impede the migration of Li ions into the core space and act as a barrier during the Li plating process. These types of non-porous hollow structures may result in indiscriminate plating and growth of Li on the exterior surfaces of the hollow structures due to detour and slow migration of Li ions into the core space. Eventually, this unstable Li plating on the exterior surfaces may cause Li dendrite growth and formation of dead Li, which occur more seriously under fast lithiation conditions.

In this study, a porous shell structure with nano-sized pores is designed and introduced into a 3D free-standing hollow carbon fiber sheet embedded with ZnO nanoparticles (NPs) to overcome the underlying problems in the Li metal anode (Scheme 1). ZnO is selected as lithiophilic material because it is cheaper and more abundant than other lithiophilic materials such as Au, Ag, and Cu [22]. The designed structure is used as a Li host framework to improve the electrochemical performance of the Li metal anode by controlling the Li plating/stripping behaviors to prevent Li dendrite growth. Pores are formed in the shell side of the hollow carbon fibers and act as a passage for the migration of Li ions into/out of the core space of the fibers where lithiophilic ZnO NPs are dispersed. The free-standing porous hollow carbon fiber sheets are fabricated by a dual-nozzle electrospinning technique followed by a carbonization step. The Li host frameworks as anode material are tested under various lithiation conditions to evaluate the

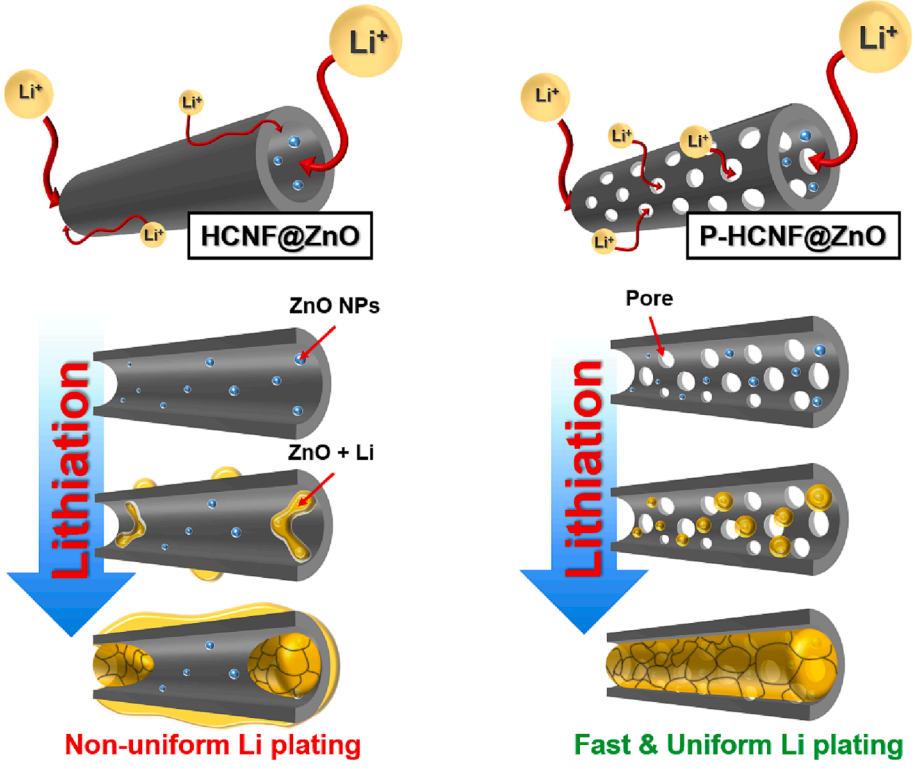

Scheme 1. Schematic representation of Li plating behaviors on the HCNF@ZnO and P-HCNF@ZnO, respectively.

effects of the pores on Li plating behaviors as well as the performance of the anode.

2. Experimental section

2.1. Materials

For the preparation of electrodes by electrospinning, polyacrylonitrile (PAN, MW = 150,000 g mol^{-1}), polymethyl methacrylate (PMMA, Mw = 120,000 g mol^{-1}), N, N-dimethylformamide (DMF, 99.8%), Polyvinylpyrrolidone (PVP, Mw = 1,300,000 g mol^{-1}), and ZnO NPs, (<50 nm) were used. For electrochemical tests, coin cell parts (CR2032) and pure Li metal foil, polypropylene (PP) separators, an electrolyte composed of 1 M lithium bis(trifluoromethanesulfonyl) imide (LiTFSI) dissolved in the solvents of 1,3-dioxolane (DOL) and 1,2-dimethoxyethane (DME) at a 1:1 vol ratio with 1 wt% lithium nitrate ($LiNO_3$) additive, LFP powder, Super P powder, polyvinylidene fluoride (PVDF, MW = 530,000 g mol^{-1}), and N-methyl-2-pyrrolidone (NMP) were used.

2.2. Fabrication of porous hollow carbon nanofibers embedded with ZnO NPs (P-HCNF@ZnO)

The HCNF@ZnO denotes a plain hollow carbon nanofiber embedded with ZnO NPs, and P-HCNF@ZnO has pores on the wall of the HCNF. For the fabrication of HCNF@ZnO, a dual nozzle was used in the electrospinning equipment, as shown in Fig. 1a. The shell-side solution was prepared by dissolving 4.5 wt% of PAN in DMF, and the core-side solution was prepared by dissolving 21 wt% of PMMA and 0.3 wt% of ZnO NPs in DMF. The mixtures were then loaded into respective syringes with a stainless-steel needle (27 G × 13 mm). Electrospinning was carried out for 3 h under a positive voltage of 15 kV, a tip-to-collector distance of 15 cm, and the jet rates of the shell and the core polymer solutions of 1.0 and 0.5 ml h^{-1}, respectively. Next, the electro-spun polymer web was dried at room temperature in a fume hood for 24 h to remove the remaining DMF, then pre-stabilization heat treatment was carried out at 150 °C for 5 h in an air atmosphere to maintain the structural stability of the PAN fibers. For further stabilization of the structure, the resulting PAN fiber web was subjected to a heating step at 250 °C for 3 h in an air atmosphere, followed by carbonization at 700 °C for 1 h under a nitrogen atmosphere in a tubular furnace. To fabricate hollow carbon fibers having pores in the walls (P-HCNF@ZnO), a given amount of PVP was added to the shell-side solution as a pore former. That is, the shell-side solution was composed of equal amounts of 4.5 wt % of PAN in DMF and 4.5 wt% of PVP in DMF. The other chemical compositions and procedures were the same as in the case of HCNF@ZnO.

2.3. Fabrication of LFP cathodes

For full cell tests, LFP cathodes were prepared using a slurry containing LFP powder, Super P powder, and PVDF that were dispersed in NMP with a weight ratio of 8:1:1. Then, the slurry was cast on an Al current collector using a doctor blade with a gap of 150 μm, and dried at 60 °C for 24 h in a vacuum drying oven.

2.4. Materials characterization

Morphologies and structures of the anode materials were analyzed using field emission-scanning electron microscopy (FE-SEM, Inspect F50) operated at 15 kV and high-resolution transmission electron microscopy (HR-TEM, FEI Tecnai F20, Tecnai) operated at 200 kV. The pore size distributions (PSDs) and Brunauer-Emmett-Teller (BET) were measured using N_2 adsorption–desorption isotherms (Micromeritics ASAP 2020) with the Barrett–Joyner–Halenda (BJH) method. The crystal structures of the electrodes were measured by X-ray diffraction (XRD, Rigaku) analysis, equipped with Cu Kα radiation (λ = 0.154 Å) at 30 kV and 15 mA at a scan rate of 2.0° m^{-1}.

2.5. Electrochemical performance tests

The anodes used for electrochemical tests were made by cutting an HCNF@ZnO or a P-HCNF@ZnO sheet into disks with a diameter of 1.2 cm^2 and are used as a free-standing electrode without ancillary components such as a binder, electric conducting additives, and current collector. All electrochemical measurements were carried out using CR2032 coin cells fabricated in a dry room with a dew point below −60 °C. All galvanostatic charge/discharge tests were conducted using a battery test system (Maccor 4300 K). Electrochemical impedance spectroscopy (EIS) was carried out using a VSP tester (Biologic, Inc.) in the frequency range of 0.1 Hz to 200 kHz. For the Coulombic efficiency (CE) tests of a half-cell, an HCNF@ZnO or a P-HCNF@ZnO was employed as the working electrode, a PP film as the separator, and a Li metal foil (~15 μm thick) as the reference and counter electrode. These cells were activated for five cycles at 0–1.0 V (vs. Li^+/Li) at 0.1 mA cm^{-2} to remove the impurity on the surface of the electrodes. Then, a pre-determined amount of Li (calculated based on the areal capacity) was plated onto the electrodes at a constant current and then stripped by charging to 1.0 V (vs. Li^+/Li) for each cycle. For the symmetrical cell tests, the electrodes were pre-lithiated by 1.0 mAh cm^{-2} of Li at 0.1 mA cm^{-2} and

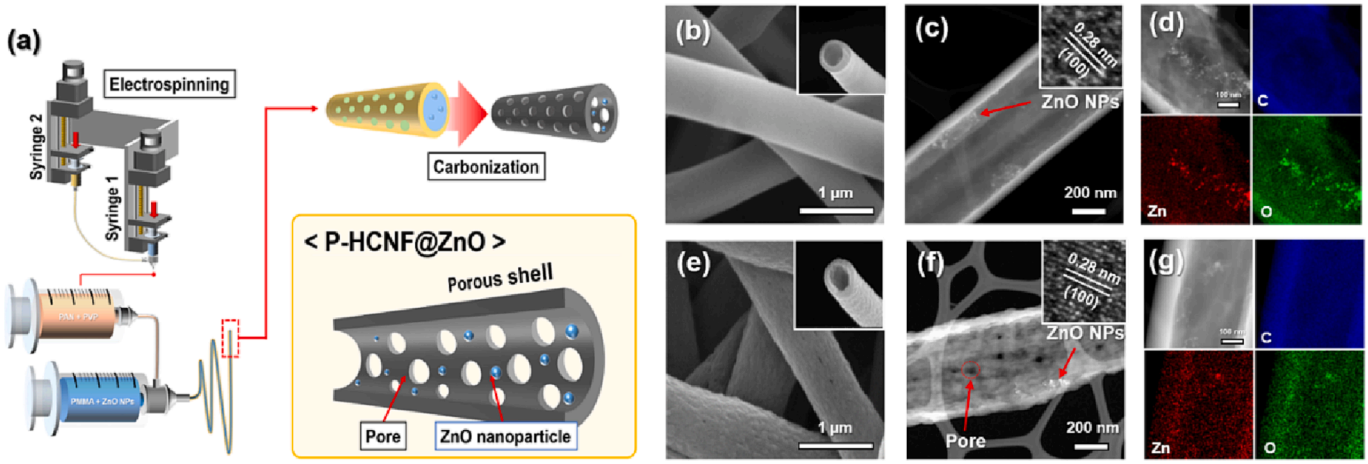

Fig. 1. (a) A schematic of the preparation process of P-HCNF@ZnO through electrospinning and carbonization. FE-SEM images of (b) HCNF@ZnO and (e) P-HCNF@ZnO. HR-TEM images of (c and d) HCNF@ZnO and (f and g) P-HCNF@ZnO. EDS mapping images of (d) HCNF@ZnO and (g) P-HCNF@ZnO.

tested at 0.05 to 0.5 mA cm^{-2} with an areal capacity of 0.2 mAh cm^{-2}. LFP full cell tests were carried out using slurry-casted electrodes as anode with Li pre-lithiated by 5.0 mAh cm^{-2} in the voltage range of 2.5–4.0 V vs. Li^{+}/Li at 0.1 C-rate to demonstrate the feasibility of P-HCNF@ZnO electrodes in a practical full cell system.

3. Results and discussion

Fig. 1a shows the fabrication process of a P-HCNF@ZnO, where an electrospinning device having a dual nozzle was used to fabricate an e-spun polymer web consisting of double-layered polymer fibers. The e-spun polymer fibers were composed of a mixture of PAN and PVP on the shell side and a PMMA solution containing ZnO NPs on the core side, which were then dried and subjected to a carbonization process. During the carbonization process, the shell-side PAN was converted to carbon, and the PVP was decomposed to leave pores in the shell side; meanwhile, the PMMA in the core side was also decomposed to leave a hole along the fiber, and the ZnO NPs were dispersed all over the surface of the core side. The non-porous HCNF@ZnO was prepared following the same procedure without the PVP in the shell-side solution.

The morphology and structure of the HCNF@ZnO and P-HCNF@ZnO were characterized using FE-SEM and HR-TEM. The SEM and TEM images of HCNF@ZnO in Fig. 1b and c show that the solid PAN fibers were transformed into hollow carbon fibers with an average diameter of about 430 nm and a shell thickness of about 44 nm. And it has a very smooth exterior surface and does not look to have any pores in the shell. In contrast, the P-HCNF@ZnO has a rugged exterior surface (the SEM image in Fig. 1e) because of the pores having a diameter of about 12 nm in the shell (the TEM image in Fig. 1f). The PSD and BET of the carbon materials were measured more accurately using a N_2 adsorption analyzer. As shown in Fig. 2, the P-HCNF@ZnO has a well-defined PSD having a prominent peak at around 2 nm and another small peak at 11 nm (average pore diameter = 9.8 nm, BET surface area = 98.1 m^2 g^{-1}). In contrast, the HCNF@ZnO appears almost non-porous, only having a minimal number of pores above 20 nm (average pore diameter = 79.2 nm, BET surface area = 15.1 m^2 g^{-1}). Regarding the ZnO NPs dispersed on the inner surface of the hollow fibers, their particle sizes are 8 ~ 20 nm (Fig. 1c), and they are uniformly distributed all over the surface, as confirmed by the EDS elemental mapping in Fig. 1d and g. They also have a characteristic lattice spacing of 0.28 nm which can be assigned to the (1 0 0) lattice of the ZnO, as shown in the insets of Fig. 1c and f [23].

To investigate the Li plating behaviors on the electrodes, the lithiation tests were conducted with a coin cell composed of an HCNF@ZnO or a P-HCNF@ZnO sheet as the working electrode and a Li foil (~15 μm thick) as the counter electrode at a constant current of 0.1 mA cm^{-2} with varying areal capacities. Fig. 3 displays the SEM images showing the Li plating status in the electrodes with increasing Li areal capacities from 0.0 to 2.0 mAh cm^{-2}. As the areal capacity increases, Li gradually plates in the core space of the hollow fiber electrode, reducing the inner diameter and finally filling the hollow space. It appears that the P-HCNF@ZnO is filled up faster than the HCNF@ZnO. In the case of the HCNF@ZnO electrode, the growth of protrusions is observed on the exterior surface of the fibers from 1.0 mAh cm^{-2} even when the hollow space is not filled (Fig. 3c). They grow much bigger at 2.0 mAh cm^{-2} (Fig. 3d). In the case of P-HCNF@ZnO electrode, Li fills the hollow space gradually, and the space is completely filled with Li at 1.0 mAh cm^{-2} (Fig. 3g). But protrusions are not formed at all even when the areal capacity is doubled to 2.0 mAh cm^{-2} to electroplate two times more amount of Li (Fig. 3h). This indicates that even after the core space of P-HCNF@ZnO is filled up, excessively plated Li is formed very uniformly on the exterior surface of the fibers without growing large Li protrusions probably because of the porous surface of the shell which may help uniformly disperse the electric charge all over the surface. This means that the Li dendrites can be almost perfectly prevented from growing on the surface of the P-HCNF@ZnO electrode [24].

Fig. 3i schematically illustrates the electroplating behaviors of Li in the hollow carbon fibers with increasing areal capacity. The formation of Li protrusions on the exterior surface of the HCNF@ZnO electrode can also be clearly observed in the photographs of the electrode taken after cycling at various areal capacities (Fig. S1), where the white spots are due to the Li plating formed on the exterior surface of the fibers and their number and size increase with increasing the areal capacity. On the other hand, in the case of P-HCNF@ZnO, the white spots of Li are rarely observed. Though there are some white spots at the highest areal

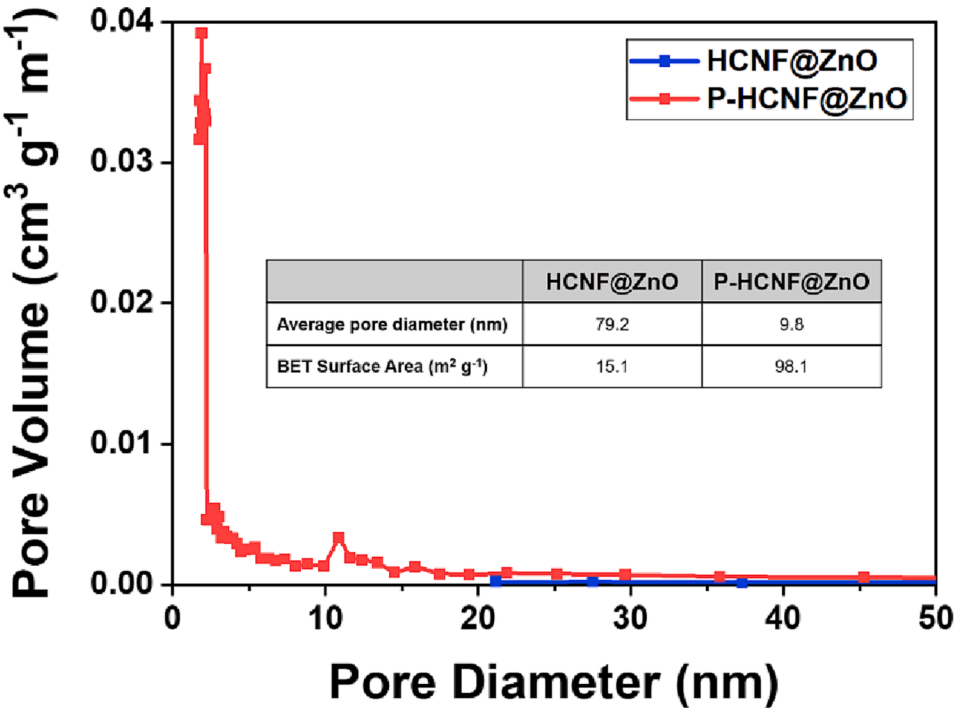

Fig. 2. PSD and BET of the carbon materials measured using a N_2 adsorption analyzer and calculated using the BJH method.

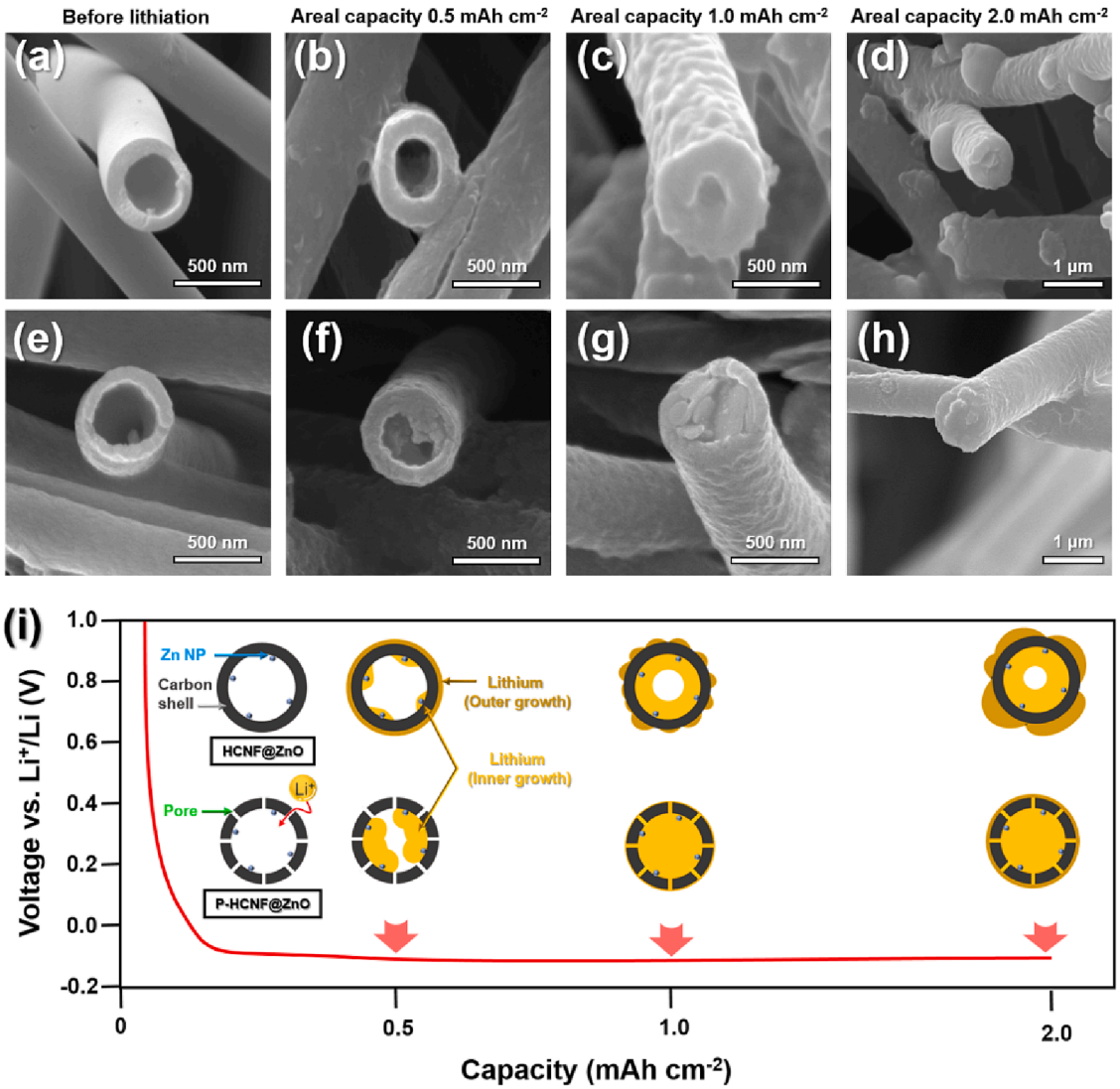

Fig. 3. SEM images of (a-d) HCNF@ZnOs and (e-f) P-HCNF@ZnOs showing Li filling inside the hollow fibers at different areal capacities of 0 (pristine), 0.5, 1.0, and 2.0 mAh cm^{-2} at a current density of 0.1 mA cm^{-2}. (i) A schematic diagram of Li plating behaviors with increasing the areal capacity.

capacity of 2.0 mAh cm^{-2}, they might not be protrusions but smooth Li layers coated on the surface of the fibers, as shown in Fig. 3h. These differences in the Li plating behaviors may be ascribed to the presence of micropores in the wall of hollow carbon fibers, which guides and facilitates the migration of Li ions into the core space and allow them to plate there. Therefore, in the case of the electrode made of porous hollow carbon fibers embedded with lithiophilic ZnO particles, Li is easily attracted into and preferentially electroplated in the core space of the carbon fiber. By this mechanism, the growth of Li dendrites on the exterior surface of the fibers is suppressed almost perfectly.

From now on, all the cell tests have been carried out by fixing the lithiation areal capacity at 1.0 mAh cm^{-2} because it is suitable for clearly showing the effects of pores in the hollow carbon fibers on the Li plating behaviors.

The effects of ZnO on the Li plating behaviors were also investigated by varying the amount of ZnO in the core space of the P-HCNF framework. Fig. S2 are the SEM images showing the morphologies of Li plating in the presence and absence of ZnO in P-HCNFs. In the absence of ZnO, the core spaces of the fibers are only partially filled with Li, but large Li clusters are formed outside of the fibers (Fig. S2a). In contrast, in the presence of ZnO (P-HCNF@ZnO), all the core spaces of the fibers become almost completely filled with Li (Fig. 3g and Fig. S2b) under an areal capacity of 1.0 mAh cm^{-2}, indicating the preferential plating of Li inside the cores in the presence of ZnO. When increasing the ZnO content in P-HCNF, a large portion of the inner space of the fibers is occupied by ZnO particles; thus, excess Li spills over and plates outside the fibers during lithiation, as shown in Fig. S3. As ZnO is not an active material for Li batteries, the smaller amount of ZnO is the better as long as it is enough to induce Li^+ inside the core space of the hollow structure. As described above, it has been verified that ZnO NPs can facilitate the diffusion of Li^+ into the core space of the hollow fibers and preferentially plate there, and thus help prevent the growth of large Li clusters and dendrites on the exterior surface of the fibers.

The effects of pores on the Li plating behaviors were investigated in more detail by testing the electrodes at various current densities of 0.1, 0.5, and 1.0 mA cm^{-2}. The over-potential elements in a typical Li plating curve shown in Fig. 4a can be divided into two parts: (1) the upper part (purple region) is composed of the elements such as mass-transfer, charge-transfer, and ohmic resistances, (2) the lower part (yellow region) is composed of the element of Li nucleation over-potential [25]. The mass-transfer resistance element in the upper part accompanies the entire process of Li plating and is influenced by the diffusion rate of Li ions and the current density. On the other hand, the nucleation over-potential in the lower part is directly affected by the Li nucleation ability of the material, which varies depending on the lithiophilic characteristics [11]. Fig. 4b-d show Li plating curves of the HCNF@ZnO

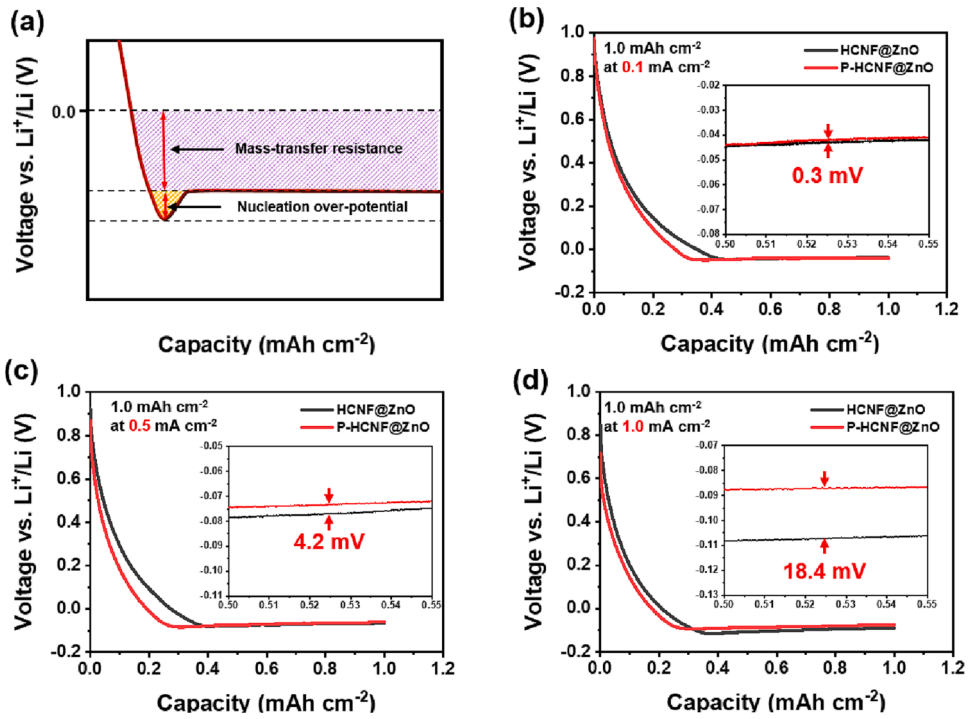

Fig. 4. (a) A typical Li plating curve showing over-potential elements. (b-d) Li plating curves for the HCNF@ZnO and the P-HCNF@ZnO electrode obtained with a Li areal capacity of 1.0 mAh cm^{-2} at various current densities; (b) 0.1, (c) 0.5, and (d) 1.0 mA cm^{-2}.

and P-HCNF@ZnO electrodes at various current densities, and the nucleation and mass-transfer over-potentials obtained from the curves are summarized in Table 1. At a current density of 0.1 mA cm^{-2} in Fig. 4b, both electrodes exhibit very similar over-potentials for the Li nucleation and mass transfer, and the difference in the mass transfer over-potentials between the electrodes is only 0.3 mV. However, as the current density is raised, the difference increases up to 4.2 mV at 0.5 mA cm^{-2} (Fig. 4c) and 18.4 mV at 1.0 mA cm^{-2} (Fig. 4d). The lower over-potentials for the P-HCNF@ZnO electrode means that the pores in the electrode contribute to the reduction of mass transfer over-potential. In the case of nucleation over-potential, both electrodes display shallow profiles and almost similar over-potential values at all current densities, which means that the pores do not have appreciable impacts on the nucleation over-potential. However, considering the over-potential values are relatively low, the lithiophilic ZnO NPs seem to contribute to the reduction of nucleation over-potential [11].

The relationship between the electrode structure and the over-potentials has been sought by comparing the morphologies of the Li plating formed on the electrodes. Fig. 5 displays the SEM images of the Li-plated HCNF electrodes obtained at current densities of 0.1, 0.5, and 1.0 mA cm^{-2} with a fixed areal capacity of 1.0 mAh cm^{-2}. It is found that the morphology of the Li plating on the electrode is greatly affected by the structure of the electrode. In the case of the HCNF@ZnO electrode, it is clearly shown that protrusions are formed on the surface of the fibers. Their number and size become bigger as the current density or the electroplating rate increases, even though the areal capacity or the total amount of plated Li is kept the same for all the samples (Fig. 5a–c). On the contrary, the P-HCNF@ZnO electrode having pores in the wall of the fibers shows very smooth surfaces, and only a few Li protrusions are observed at the highest current density of 1.0 mA cm^{-2} (Fig. 5d–f). This means that most of the Li ions migrate into the core space of the hollow fibers through the pores in the walls and are uniformly electroplated inside the cores. Comparing the SEM images of the two types of electrodes, it is clear that the formation of Li protrusions is almost completely prevented for the P-HCNF@ZnO electrodes, indicating that the pores play a decisive role in inhibiting the growth of Li protrusions on the surface of the hollow carbon fibers. This is because the formation of Li protrusions on the exterior surface is directly related to the relative speed of the Li plating (i.e., the current density) versus the mass-transfer rate of Li into the cores even though the total amounts of Li to be electroplated are kept the same. If the Li plating rate is higher than the mass-transfer rate of Li ions into the core space, the Li protrusions grow on the

Table 1
Li nucleation and mass-transfer over-potentials of the electrodes at various Li areal capacities taken from Fig. 4.

		Over-potential		
		At 0.1 mA cm^{-2}	At 0.5 mA cm^{-2}	At 1.0 mA cm^{-2}
Mass-transfer Resistance	**HCNF@ZnO**	**36.1 mV**	**78.7 mV**	**107.7 mV**
	P-HCNF@ZnO	36.4 mV	74.5 mV	89.3 mV
Nucleation resistance	**HCNF@ZnO**	9.2 mV	13.5 mV	27.4 mV
	P-HCNF@ZnO	9.2 mV	15.3 mV	20.0 mV

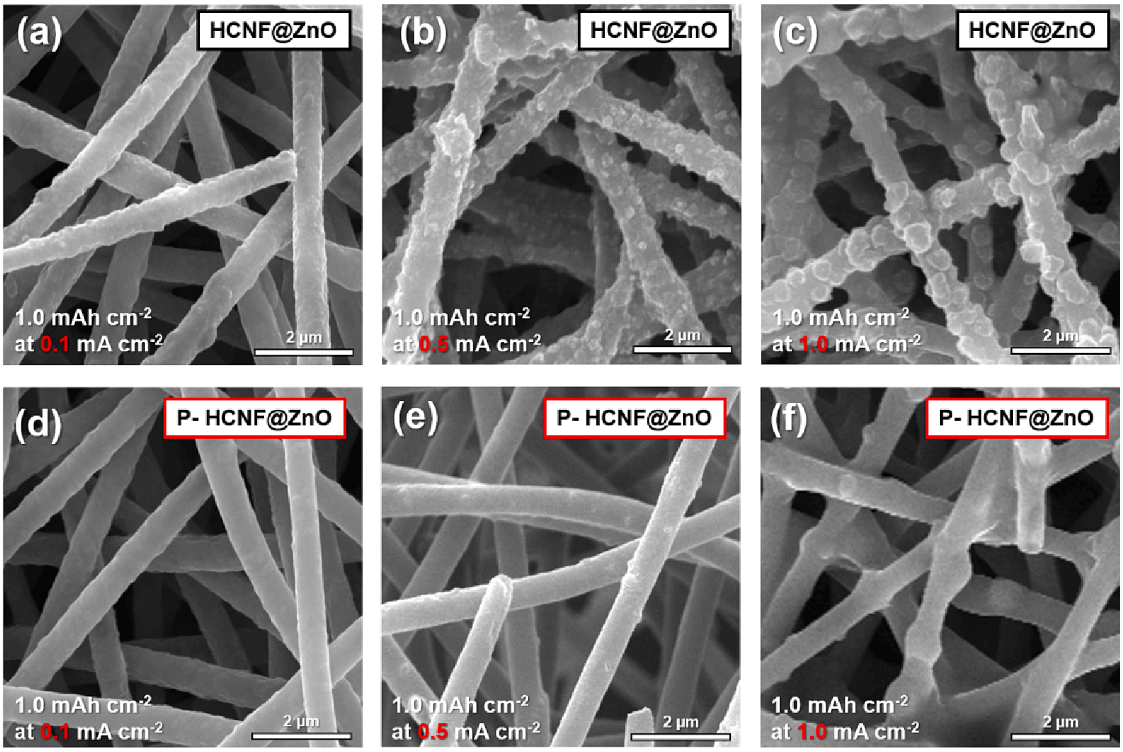

Fig. 5. FE-SEM images of Li plating behaviors on the HCNF@ZnO and P-HCNF@ZnO at different current densities; 0.1 (a and d), 0.5 (b and e), and 1.0 mA cm^{-2} (c and f).

exterior surface of the fibers. In contrast, if the mass-transfer rate to the core space is faster, most of the Li ions can migrate into the cores and are plated there without the formation of protrusions on the exterior surface. Therefore, it is evident that the pores contribute to the uniform electroplating of Li inside the cores of hollow fibers, preventing the growth of Li dendrites on the exterior surface and suppressing side reactions. Thus it can improve the battery's performance by reducing the over-potentials of the electrode.

The positive effect of the porous hollow carbon fibers is also supported by the impedance analysis. Fig. 6 shows the Nyquist plots for the HCNF@ZnO and P-HCNF@ZnO electrodes. The P-HCNF@ZnO exhibits a semicircle with a slightly smaller diameter in the high- to the medium-frequency region and a larger slope in the low frequency region than those of the HCNF@ZnO, indicating that the former has a lower charge transfer resistance and a faster mass transfer rate than those of the latter [26].

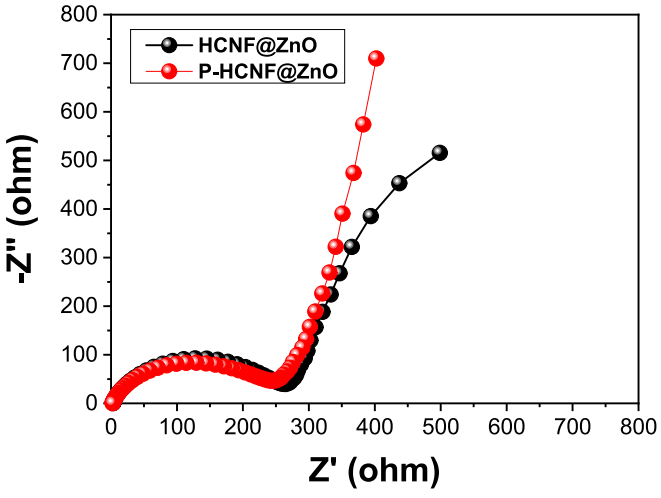

Fig. 6. Electrochemical impedance spectra of the electrodes made of a pristine HCNF@ZnO and a P-HNCF@ZnO, respectively.

To further evaluate the effects of pores on the stability and electrochemical performance during the Li plating/stripping cycles, the CEs and cycling performance of the cells employing the HCNF@ZnO or P-HCNF@ZnO electrodes were measured at various current densities. In this experiment, a fixed Li areal capacity of 1.0 mAh cm^{-2} was applied to the cell with an upper cut-off voltage of 1.0 V vs. Li^{+}/Li. Detailed voltage profiles at the 10th, 30th, and 50th cycles are compared in Fig. 7. The CE is defined as the Li stripping capacity divided by the Li plating capacity for each cycle, which is an index indicating the stability of the Li metal anode during cycles. Fig. 7a–c shows the CEs of the cells employing an HCNF@ZnO and a P-HCNF@ZnO electrode, respectively, at current densities of 0.1, 0.5, and 1.0 mA cm^{-2}. Both cells show high CEs of about 98% at the current densities up to 0.5 mA cm^{-2}, as shown in Fig. 7a and b. When the current density is raised to 1.0 mA cm^{-2} (Fig. 7c), the P-HCNF@ZnO maintains a high CE of about 95%, but the CE of HCNF@ZnO drops to 85% after 50 cycles, presumably because of the irreversible property of the excessively plated Li on the outside of HCNF@ZnO electrode that may form dead Li particles. Fig. 7d–i show detailed Li plating/stripping curves for HCNF@ZnO and P-HCNF@ZnO electrodes. The over-potential calculated from the difference between the plateaus of the stripping and the plating curves increases with the current density. As the current density increases from 0.1 to 1.0 mA cm^{-2}, the over-potential rises from 18 to 112 mV for the HCNF@ZnO while it rises from 18 to 87 mV for the P-HCNF@ZnO. Overall, the over-potentials of the P-HCNF@ZnO are smaller than those of the HCNF@ZnO, and the discrepancy between them increases with increasing the current density. In addition, the P-HCNF@ZnO shows higher capacities than the HCNF@ZnO. When comparing the curves recorded at the 10th, 30th, and 50th cycles, the capacity of the HCNF@ZnO appears to increase as the cycle progresses, probably because of the activation of the core space of the hollow carbon fibers that could provide more sites for the electroplating of Li. In the case of P-HCNF@ZnO, the differences in the capacities among the cycles are much

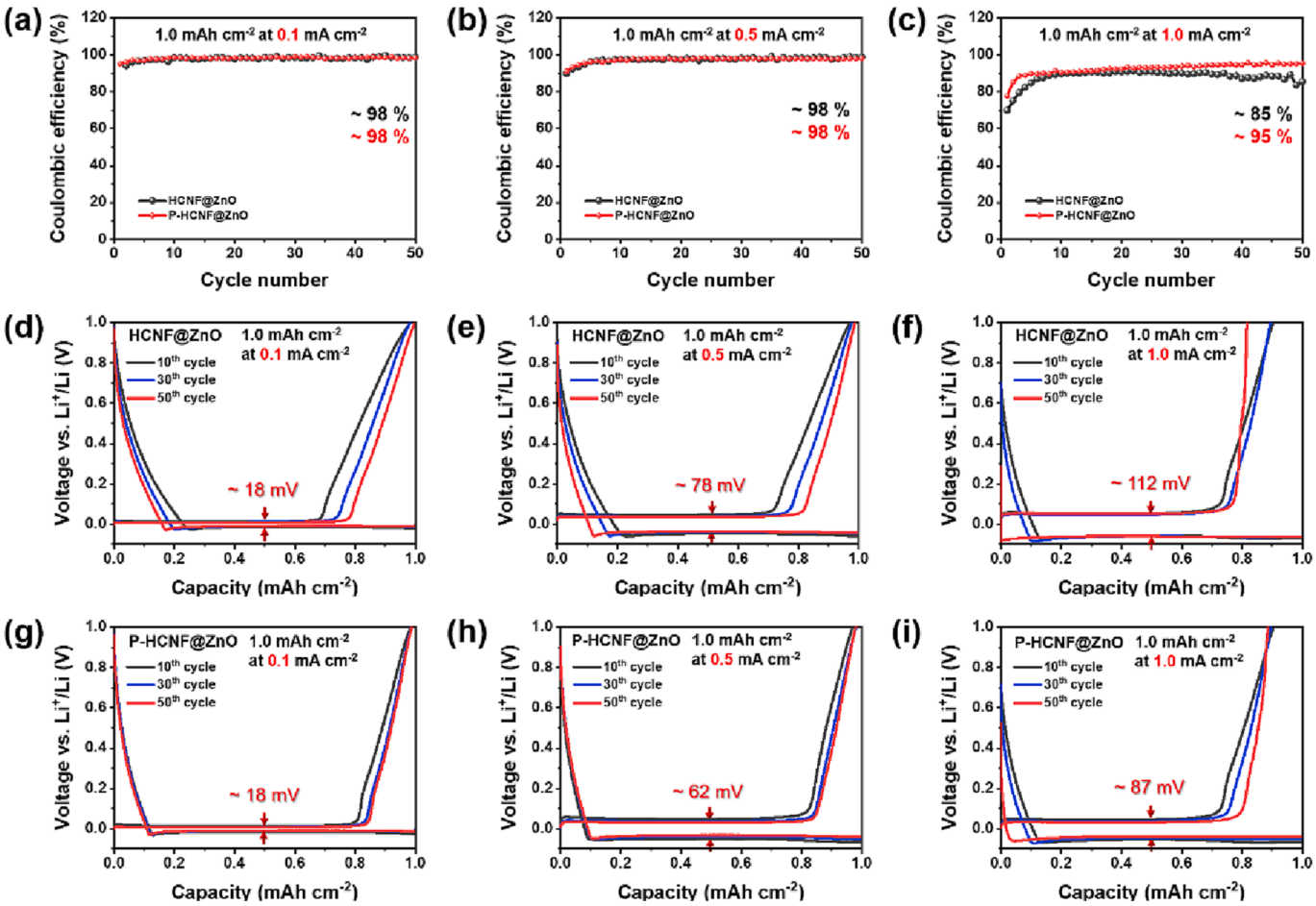

Fig. 7. Coulombic efficiencies of the HCNF@ZnO and P-HCNF@ZnO with a Li areal capacity of 1.0 mAh cm^{-2} at various current densities; (a) 0.1, (b) 0.5, and (c) 1.0 mA cm^{-2}. The detailed voltage profiles at the 10th, 30th, and 50th cycles at (d and g) 0.1, (e and h) 0.5, and (f and i) 1.0 mA cm^{-2}.

smaller than those of the HCNF@ZnO. This may be ascribed to the uniform and efficient Li plating/stripping behaviors induced by the fast mass-transfer of Li ions to the core space of the carbon fibers through the pores. In view of Fig. 7f, vertical Li plating/stripping voltage curves are observed at the 50th cycle, which resembles the behavior of the Li-metal electrode. This kind of phenomenon occurs when the electrode is completely covered with Li metal, as shown in Fig. 5c, which causes a fast Li plating/stripping cycling almost in the absence of mass transfer limitation [14]. A similar but less steep vertical curve is also observed for the P-HCNF@ZnO at 1.0 mA cm^{-2} in Fig. 7i.

Fig. S4 shows the SEM images of the electrodes after the 1st and the 50th cycle. In the case of the HCNF@ZnO electrode, many Li protrusions or clusters are observed on the surfaces of fibers even after the 1st cycle (Fig. S4a), and the Li clusters on the surfaces become dead Li as a result of 50 cycles of repeated Li plating/stripping processes (Fig. S4b). On the contrary, in the case of the P-HCNF@ZnO electrode, the surfaces of the carbon fibers look very clean after the 1st cycle (Fig. S4c), and the formation of Li protrusions is scarce even after 50 cycles (Fig. S4d). This shows the effects of the pores in the wall of carbon fibers that enable stable and uniform plating/stripping of Li during the cycles and thus enhance the long-term performance of the battery even under high current density conditions by suppressing the formation of Li dendrites.

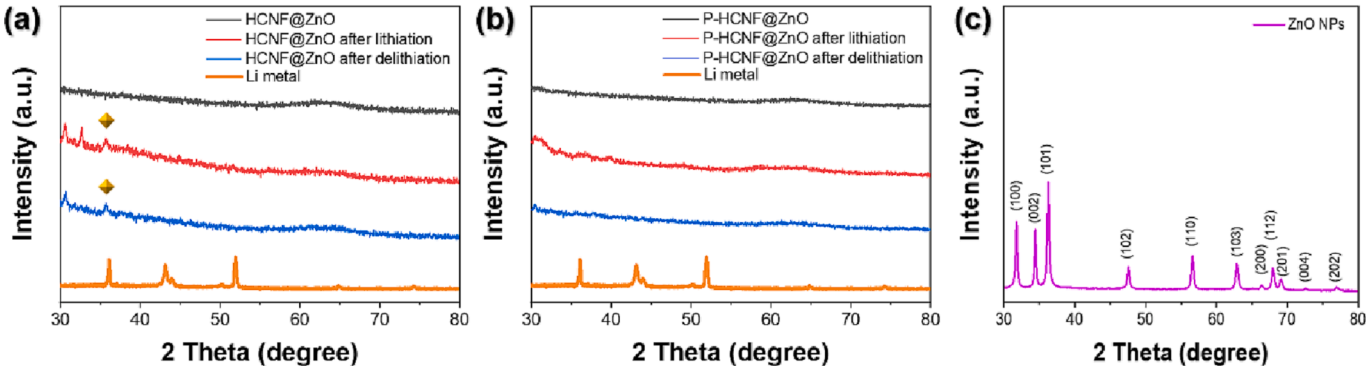

Fig. 8. XRD patterns of (a) HCNF@ZnO and (b) P-HCNF@ZnO after lithiation and delithiation at the first cycle, and (c) pure ZnO NPs. The yellow diamond indicates the peaks related to the Li. (For interpretation of the references to colour in this figure legend, the reader is referred to the web version of this article.)

The difference in Li plating behaviors between HCNF@ZnO and P-HCNF@ZnO during lithiation and delithiation can also be confirmed by XRD data in Fig. 8. The XRD pattern of HCNF@ZnO after lithiation shows a Li peak at 5.69°, whereas Li peaks are not found in the pattern of P-HCNF@ZnO. This may be because the Li plated on the exterior surface of HCNF@ZnO forms large clusters enough to have a crystallinity. And the Li peak does not disappear even after delithiation, presumably because part of the Li clusters on the surface remains unused. This phenomenon is continually repeated during the cycles and may contribute to forming Li dendrites and dead Li particles. In the case of P-HCNF@ZnO, Li peaks are not detected. This may be because the Li plated inside the core spaces of the fibers are very small and could not grow enough to have a crystallinity [27]. In the case of ZnO, it has a typical XRD pattern, as shown in Fig. 8c, which is obtained from pure ZnO particles. However, in the XRD patterns of HCNF@ZnO and P-HCNF@ZnO, ZnO peaks are not seen, probably because the amount of ZnO NPs in the hollow fibers is too small to be detected, and they are surrounded by carbon shells.

The symmetric cell test provides a valuable platform for quantitatively evaluating Li metal anode performance without decoupling cathode effects. Before the symmetric cell tests, the HCNF@ZnO and P-HCNF@ZnO sheets were pre-lithiated with Li under an areal capacity of 1.0 mAh cm^{-2} to make lithiated electrodes. Then, the symmetric cell tests were conducted at a fixed Li areal capacity of 0.2 mAh cm^{-2} while increasing the current density from 0.05 to 0.5 mA cm^{-2} to compare the stability of the electrodes. Fig. 9 shows the voltage profiles during Li plating/stripping cycles at two different current densities for the symmetric cells using HCNF@ZnO and P-HCNF@ZnO electrodes, respectively. At 0.05 mA cm^{-2}, the voltage profiles of the two electrodes look very similar, but in view of the magnified ones in Fig. 9b, the HCNF@ZnO exhibits a higher over-potential by 13.1 mV than P-HCNF@ZnO. It also displays peaking shape voltage curves at the profile's upper corners, indicating indiscriminate Li plating/stripping at the Li clusters formed on the exterior surface [28]. When the current density is increased to 0.5 mA cm^{-2}, the HCNF@ZnO exhibits a much sharper voltage curve, of which amplitude rises to 1.0 V in 32 h as the cycle progresses. In contrast, the P-HCNF@ZnO shows a very stable profile with a low over-potential because the pores in the hollow carbon fibers enable fast and uniform Li plating/stripping processes.

To demonstrate the feasibility of P-HCNF@ZnO as an anode, LFP full cell tests were conducted using the anodes prepared by a slurry-casting method described in the experimental section. Before full cell tests, the anodes were lithiated through pre-lithiation with a 5.0 mAhcm^{-2} of Li areal capacity. These lithiated HCNF@ZnO and P-HCNF@ZnO were named Li@HCNF@ZnO and Li@P-HCNF@ZnO. As shown with the charge–discharge profiles of the LFP full cells at 0.1C in Fig. S5, the Li@P-HCNF@ZnO|LFP shows a higher specific capacity and a lower over-potential than those of Li@HCNF@ZnO|LFP. These results demonstrate the enhanced performance of the battery with P-HCNF@ZnO electrodes.

4. Conclusion

In this study, free-standing P-HCNF@ZnO sheets consisting of porous hollow carbon fibers embedded with lithiophilic ZnO NPs were successfully fabricated using a dual-nozzle electrospinning technique followed by carbonization to develop Li host frameworks for highly stable and efficient lithium metal anodes. Through many trial-errors and optimization of the fabrication conditions, we could have succeeded in establishing a method to make porous hollow carbon fibers embedded with lithiophilic ZnO NPs. The nano-sized pores formed in the shell of the hollow carbon fiber provide passages for Li ions to migrate into the core space and plate there. In the case of the non-porous HCNF@ZnO electrode, many large-size Li dendrites and clusters are formed on the fiber's exterior surface because only a small portion of Li ions could move into the core space of the fibers. On the other hand, in the case of the P-HCNF@ZnO electrode, the nano-sized pores formed in the shell of hollow carbon fibers provide passages for Li ions to penetrate to the core space of the hollow fibers and plate there efficiently and uniformly. It is also found that the preferential plating of Li inside the cores is found to be mainly due to the presence of ZnO particles. Furthermore, even when the amount of plated Li is too large for the core space of the fiber, the excess Li is electroplated uniformly on the exterior surface of the P-HCNF@ZnO, so the growth of Li protrusions or dendrites is almost perfectly prevented. Even under fast electroplating conditions, no noticeable growth of dendrites on the surface of P-HCNF@ZnO is observed. These advantages are confirmed with symmetric and full cell systems employing the P-HCNF@ZnO anodes. In a symmetric cell test, the P-HCNF@ZnO shows a lower over-potential and higher cyclic performance than the HCNF@ZnO. Similar results are also observed in full cell tests; the P-HCNF@ZnO battery outperforms the HCNF@ZnO battery in capacity and over-potential.

In conclusion, it is confirmed that the P-HCNF@ZnO could almost perfectly suppress the growth of Li dendrites by inducing the Li electroplating preferentially inside the core space of the hollow carbon fibers. Therefore, the porous hollow carbon nanofibers embedded with lithiophilic ZnO particles could be a promising Li host framework for stable and highly performing Li metal anodes.

Declaration of Competing Interest

The authors declare that they have no known competing financial

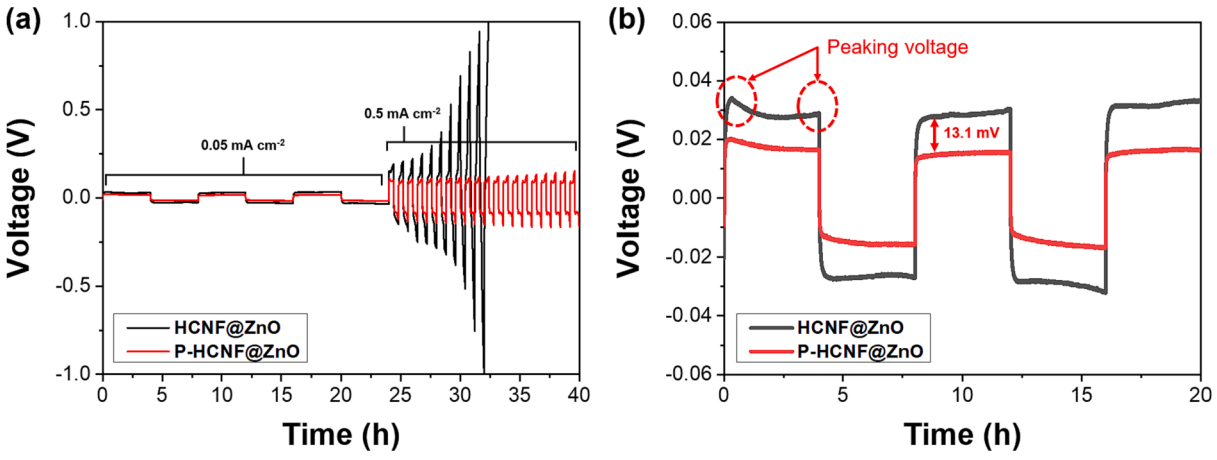

Fig. 9. (a) Voltage curves of the symmetric cells employing an HCNF@ZnO and a P-HCNF@ZnO electrode, respectively, at the current densities of 0.05 and 0.5 mA cm^{-2} under a fixed areal capacity of 0.2 mAh cm^{-2}. (b) Magnified voltage curves recorded for 20 h at a current density of 0.05 mA cm^{-2}.

interests or personal relationships that could have appeared to influence the work reported in this paper.

Data availability

Data will be made available on request.

Acknowledgment

This work was supported by the institutional program of the Korea Institute of Science and Technology (KIST, Project No. 2E32582).

Appendix A. Supplementary data

Supplementary data to this article can be found online at https://doi.org/10.1016/j.cej.2023.142713.

References

[1] S. Chen, F. Dai, M. Cai, Opportunities and challenges of high-energy lithium metal batteries for electric vehicle applications, ACS Energy Lett. 5 (2020) 3140–3151.
[2] M. Rana, S.A. Ahad, M. Li, B. Luo, L. Wang, I. Gentle, R. Knibbe, Review on areal capacities and long-term cycling performances of lithium sulfur battery at high sulfur loading, Energy Storage Mater. 18 (2019) 289–310.
[3] M. Park, H. Sun, H. Lee, J. Lee, J. Cho, Lithium-air batteries: survey on the current status and perspectives towards automotive applications from a battery industry standpoint, Adv. Energy Mater. 2 (2012) 780–800.
[4] P. Shi, X.-Q. Zhang, X. Shen, R. Zhang, H. Liu, and Q. Zhang, A review of composite lithium metal anode for practical applications, Adv. Mater. Technol. 5 (202) 19008061900807.
[5] J. Wang, B. Ge, H. Li, M. Yang, J. Wang, D. Liu, C. Fernandez, X. Chen, Q. Peng, Challenges and progresses of lithium-metal batteries, Chem. Eng. J. 420 (2021) 129739.
[6] N.W. Li, Y.X. Yin, C.P. Yang, Y.G. Guo, An artificial solid electrolyte interphase layer for stable lithium metal anodes, Adv. Mater. 28 (2016) 1853–1858.
[7] F. Ding, W. Xu, G.L. Graff, J. Zhang, M.L. Sushko, X. Chen, Y. Shao, M. H. Engelhard, Z. Nie, J. Xiao, X. Liu, P.V. Sushko, J. Liu, J.-J. Zhang, Dendrite-free lithium deposition via self-healing electrostatic shield mechanism, J. Am. Chem. Soc. 135 (2013) 4450–4456.
[8] X.-B. Cheng, C.-Z. Zhao, Y.-X. Yao, H. Liu, Q. Zhang, Recent advances in energy chemistry between solid-state electrolyte and safe lithium-metal anodes, Chemistry 5 (2019) 74–96.
[9] X.-B. Cheng, M.-Q. Zhao, C. Chen, A. Pentecost, K. Maleski, T. Mathis, X.-Q. Zhang, Q. Zhang, J. Jiang, Y. Gogotsi, Nanodiamonds suppress the growth of lithium dendrites, Nat. Commun. 8 (2017) 1–9.
[10] Q. Meng, B. Deng, H. Zhang, B. Wangm, W. Zhang, Y. Wen, H. Ming, X. Zhu, Y. Guan, Y. Xiang, M. Li, G. Cao, Y. Yang, H. Peng, H. Zhang, Y. Huang, Heterogeneous nucleation and growth of electrodeposited lithium metal on the basal plane of single-layer graphene, Energy Storage Mater. 16 (2019) 419–425.
[11] K. Yan, Z. Lu, H.-W. Lee, F. Xiong, P.-C. Hsu, Y. Li, J. Zhao, S. Chu, Y. Cui, Selective deposition and stable encapsulation of lithium through heterogeneous seeded growth, Nat. Ener. 1 (2016) 16010.
[12] C. Chen, J. Guan, N.W. Li, D. Luan, C.H. Zhang, G. Cheng, L. Yu, X.W.(D.) Lou, Lotus-root-like carbon fibers embedded with Ni–Co nanoparticles for dendrite-free lithium metal anodes, Adv. Mater. 33 (2021) 2100608.
[13] H. Jiang, Y. Zhou, C. Guan, M. Bai, F. Qin, M. Yi, J. Li, B. Hong, Ion/electron redistributed 3D flexible host for achieving highly reversible Li metal batteries, Small 18 (2022) 2107641.
[14] H. Yu, Y. Zeng, N. W. Li, D. Luan, L. Yu, and X. W. (D.) Lou, Confining Sn nanoparticles in interconnected N-doped hollow carbon spheres as hierarchical zincophilic fibers for dendrite-free Zn metal anodes, Sci. Adv. 8 (2022) eabm5766.
[15] S. Wang, Y. Wang, Y. Song, J. Zhang, X. Jia, J. Yang, D. Shao, Y. Li, J. Liao, H. Song, Synergistic regulating of dynamic trajectory and lithiophilic nucleation by Heusler alloy for dendrite-free Li deposition, Energy Storage Mater. 50 (2022) 505–513.
[16] C.P. Yang, Y.X. Yin, S.F. Zhang, N.W. Li, Y.G. Guo, Accommodating lithium into 3D current collectors with a submicron skeleton towards long-life lithium metal anodes, Nat. Commun. 6 (2015) 8058.
[17] G. Zheng, S.W. Lee, Z. Liang, H.-W. Lee, K. Yan, H. Yao, H. Wang, W. Li, S. Chu, Y. Cui, Interconnected hollow carbon nanospheres for stable lithium metal anodes, Nat. Nanotechnol. 9 (2014) 618–623.
[18] Z. Liang, D. Lin, J. Zhao, Z. Lu, Y. Liu, C. Liu, Y. Lu, H. Wang, K. Yan, X. Tao, Y. Cui, Composite lithium metal anode by melt infusion of lithium into a 3D conducting scaffold with lithiophilic coating, Proc. Natl. Acad. Sci. U S A 113 (2016) 2862–2867.
[19] Z. Guo, Q. Zhang, C. Wang, Y. Zhang, S. Dong, G. Cui, I-containing polymer/alloy layer-based Li anode mediating high-performance lithium-air batteries, Adv. Funct. Mater. 23 (2022) 2108993.
[20] P. X. Sun, Z. Cao, Y. X. Zeng, W. W. Xie, N. W. Li, D. Luan, S. Yang, L. Yu, and X. W. (D.) Lou, Formation of Super-Assembled TiOx/Zn/N-Doped Carbon Inverse Opal Towards Dendrite-Free Zn Anodes, Angew. Chem. 61 (2022) e202115649.
[21] B.G. Kim, D.W. Kang, G. Park, S.H. Park, S.-M. Lee, J.W. Choi, Electrospun Li-confinable hollow carbon fibers for highly stable Li-metal batteries, Chem. Eng. J. 422 (2021) 130017.
[22] D. Zhang, A. Dai, M. Wu, K. Shen, T. Xiao, G. Hou, J. Lu, Y. Tang, Lithiophilic 3D Porous CuZn Current Collector for Stable Lithium Metal Batteries, ACS Energy Lett. 5 (2020) 180–186.
[23] P. Jamdagni, J.S. Rana, P. Khatri, K. Nehra, Comparative account of antifungal activity of green and chemically synthesized zinc oxide nanoparticles in combination with agricultural fungicides, Int. J. Nano Dimens. 9 (2018) 198–208.
[24] H. Zhang, X. Liao, Y. Guan, Y. Xiang, M. Li, W. Zhang, X. Zhu, H. Ming, L. Lu, J. Qiu, Y. Huang, G. Cao, Y. Yang, L. Mai, Y. Zhao, H. Zhang, Lithiophilic-lithiophobic gradient interfacial layer for a highly stable lithium metal anode, Nat. Commun. 9 (2018) 3729.
[25] X.L. Zhang, Z.-Q. Ruan, Q.-T. He, X.-J. Hong, X. Song, Q.-F. Zheng, J.-H. Nie, Y.-P. Cai, H. Wang, Three-Dimensional (3D) Nanostructured Skeleton Substrate Composed of Hollow Carbon Fiber/Carbon Nanosheet/ZnO for Stable Lithium Anode, ACS Appl. Mater. Interfaces 13 (2021) 3078–3088.
[26] I. Yang, S.-G. Kim, S.H. Kwon, M.-S. Kim, J.C. Jung, Relationships between pore size and charge transfer resistance of carbon aerogels for organic electric double-layer capacitor electrodes, Electrochim. Acta 223 (2017) 21–30.
[27] K.-H. Chen, K.N. Wood, E. Kazyak, W.S. LePage, A.L. Davis, A.J. Sanchez, N. P. Dasgupta, Dead lithium: mass transport effects on voltage, capacity, and failure of lithium metal anodes, J. Mater. Chem. A 5 (2017) 11671–11681.
[28] S.M. Londono-Restrepo, R. Jeronimo-Cruz, B.M. Millan-Malo, E.M. Rivera-Munoz, M.E. Rodriguez-Garcia, Effect of the Nano Crystal Size on the X-ray Diffraction Patterns of Biogenic Hydroxyapatite from Human, Bovine, and Porcine Bones, Sci. Rep. 9 (2019) 5915.